Enhancing the performance of quantum dot solar cells through halogen adatoms on carboxyl edge-functionalized graphene quantum dots

Ali A. Rajhi [a], Karam Myaser Abd Alaziz [b], Byron Stalin Rojas Oviedo [c], Anupam Yadav [d], Eduardo Hernández [e], César Gallegos [e], Sagr Alamri [f], Alaauldeen A. Duhduh [f]

[a] Department of Mechanical Engineering, College of Engineering, King Khalid University, Abha 61421, Saudi Arabia
[b] Department of Pharmacy, Al-Noor University College, Nineveh, Iraq
[c] Escuela Superior Politécnica de Chimborazo (ESPOCH), Grupo de Investigación GITAFEC, Riobamba, 060155, Ecuador
[d] Department of Computer Engineering and Application, GLA University, Mathura 281406, India
[e] Facultad Mecánica, Escuela Superior Politécnica de Chimborazo (ESPOCH), Riobamba 060155, Ecuador
[f] Department of Mechanical Engineering Technology, CAIT, Jazan University, Prince Mohammed Street, P.O. Box 114, Jazan 45142, Saudi Arabia

ARTICLE INFO

ABSTRACT

This research has been conducted to find new, high-performing, safe, and suitable materials for use in quantum dot solar cells (QDSCs). Specifically, impact of halogen adatoms (Br, Cl, and F) on carboxyl edge-functionalized graphene quantum dot (CO_2H-GQD) has been investigated employing DFT-based first-principles computations. We analyzed energy gaps (E_g), LUMO, and HOMO to determine how the foreign atom affects electronic features of material, employing hybrid functional B3LYP with a 6-31G basis set. In order to investigate charge separation and electron injection in both doped and undoped CO_2H-GQD, we examined charge transfer (CT), molecular electrostatic potential (MESP), and binding mechanism. Optical attributes also indicate a wide spectrum in visible range, making it suitable for harvesting solar light. Furthermore, we evaluated solar cell parameters, including efficiency (η), short circuit current density (J_{sc}), fill factor (FF), and open circuit voltage (V_{oc}) to assess potential usage of adatom-doped CO_2H-GQD in quantum dot solar cell. Subsequent to Br, Cl, and F substitutional doping, value of η for CO_2H-GQD increased. In case of F doping, we achieved maximum η, which has electron-donating nature and a larger radius, allowing it to inject more electrons into titanium dioxide (TiO_2) surface. Based on our research, we have determined that these recently discovered sensitizers built upon GQD exhibit considerable potential for use in QDSCs.

1. Introduction

Third-generation photovoltaic (PV) technology is increasingly seen as the most viable solution for meeting world's huge demand for green energy, thanks to its ability to generate electricity and cost-effectiveness [1–8]. QDSCs are emerging as a leading novel category of affordable solar cells, primarily because of remarkable features such as a high absorption coefficient, as well as tunable gaps that can be adjusted for size and shape [9–19]. Solar cells based on CdTe and CdSe quantum dots, cesium lead iodide ($CsPbI_3$), and colloidal lead sulfide (PbS) are widely employed in QDSCs, owing to their potential to exceed the Shockley-Queisser limit and their optical attributes that are dependent on size [20–28]. Although QDSCs have achieved high levels of efficiency, they contain toxic metals such as Cd and Pb. As a result, there is an urgent need for development of environmentally-friendly, biocompatible, and low-toxicity alternatives for production of solar cells. To in-

vestigate important attributes of QDSCs, three device configurations were examined: (a) QDSCs, which operate on principle of PV impact taking place among a metal oxide semiconductor (with a broad bandgap), QD and a redox electrolyte, (b) organic solar cells, in which PV impact arises between QD-polymer junction, and (c) Schottky junction solar cells, in which PV impact takes place between metal and QD junction [10,29–37].

QDSCs are similar in some ways to dye-sensitized solar cells (DSSCs), with main difference being that in DSCs, PV impact occurs among redox electrolyte, metal oxide semiconductor, and dye. Nevertheless, QDSCs have garnered significant attention as a potential option for solar cells. GQDs, which belong to zero-dimensional category of graphene-based materials, have been extensively investigated because of their exceptional and important attributes in bio-imaging, light emission, optoelectronics, and energy applications [38]. Their biocompatible, highly stable, and non-toxic features have made them a subject of

great interest in research community, particularly for their potential use in DSSCs [38]. Their suitability for solar cell purposes is attributed to their exceptional light-harvesting properties, size-dependent band gap tuning, edge effects, and quantum confinement. Consequently, solar cells based on variety of carbon dots (CDs) and GQDs were reported [39]. So far, GQDs have been employed in various roles such as a hole transport layer (HTL) material, in semiconductor/ graphene quantum dots, and in heterojunction solar cells. In a study by Zhang et al. [40] a power conversion efficiency (PCE) of 0.13 % was achieved using N-doped CDs. In a recent research, Wang et al. [41] developed a solar cell employing N-doped CDs and achieved a power conversion efficiency of 0.79 %. However, there is still a need to improve PCE of quantum dot solar cells. Additionally, impact of four heteroatoms over optical and electronic attributes of GQDs was studied [42]. Including heteroatoms in doping process can be an efficacious approach to manipulate electron transfer and optical attributes of GQDs by causing electronic and structural distortions. Doping foreign atoms can alter electrical distribution of GQDs, leading to tuning of their optical and electronic attributes.

Inspired by aforementioned information, we conducted a study on F, Cl, and Br-doped CO_2H-functionalized GQDs employing DFT-based first-principles methods to investigate their solar cell parameters and electronic features. Our approach involved substitution of a single C atom in carboxyl-functionalized GQD with Br, Cl, or F in order to enhance its performance, optical absorption, electronic features, and structural attributes in QDSC applications.

2. Computational method

This research utilizes DFT computations to examine impact of three adatoms (F, Cl, and Br) on CO_2H-GQD doping for QDSC use. We optimized geometry of both doped and undoped GQDs employing hybrid functional B3LYP [43–45] with a 6-31G basis set in GAMESS software [46]. Computations of vibrational frequencies is utilized to confirm if structures are stable and do not possess imaginary frequencies. Additionally, in order to achieve precision in procedure, structures were re-optimized for single-point computation using identical levels of theory in both doped and undoped systems. Using Gauss View program, we have visualized energy gap (E_g), LUMO, and LUMO. Subsequent to conducting optimization, to investigate UV–vis absorption spectra and electronic transitions, time-dependent DFT (TD-DFT) calculations were employed within integral equation formalism model (IEFPCM). Self-consistent reaction field (SCRF) approach was utilized via Polarizable Continuum Model (PCM) to account for solvent impacts in computation. PCM performs a reaction field computation employing integral equation formalism model (IEFPCM) [47]. IEFPCM creates a cavity around solute through a set of overlapping spheres. This model considers solvent impacts by utilizing macroscopic attributes such as dielectric constant (ε) and surface tension of solvent. We used water with a ε value of 78.3 at 298 K as a solvent. By comparing the maximum theoretical absorption values of quantum dots in water and using different functions for the calculation of this, we accurately determined the absorption of quantum dot graphene oxide. The calculated values are lower than the experimental value but with small variations. The range of differences between the calculated results is only about 10 nm, which is negligible and indicates that all functionals can efficiently reproduce experimental observations. However, the B3LYP hybrid functional provided the best matching result with the experimental data, with the least percentage deviation [48]. Polarization of solvent is determined by surface charge density over cavity surface, which produces an electric field that affects solute [49]. UV–vis spectra have been computed with water as solvent and impact of both undoped and doped GQDs on QDSCs have been assessed by computing solar cell parameters, including efficiency (η), short circuit current density (J_{sc}), fill factor (FF), and open circuit voltage (V_{oc}). Solar cell efficiency (η) is computed as below [50]:

$$\eta = \frac{FF J_{sc} V_{oc}}{P_{in}} \tag{1}$$

Following equations are employed to compute other parameters such as theoretical J_{sc}, FF, and V_{oc} [51]:

$$V_{oc} = E_{LUMO}^{GQDs} - E_{CB}^{TiO_2} \tag{2}$$

V_{oc} is the highest voltage that a solar cell can produce when there is no current flowing. Eq. (2) gives V_{oc} as the energy difference between conduction band (CB) of acceptor (TiO_2) and LUMO of donor (GQDs). It is also dependent on both light-generated current and saturation current, as well as it is a measure of quantity of recombination that occurs in device.

$$FF = \frac{\vartheta_{oc} - \ln(\vartheta_{oc} + 0.72)}{\vartheta_{oc} + 1}; \ \vartheta_{oc} = \frac{q \times V_{oc}}{k_B T} \tag{3}$$

The fill factor (FF) of a solar cell is a measure of maximum power output that a designed device can produce. It is related to both short-circuit current (I_{sc}) and Voc. It can be computed using Eq. (3), where υ_{oc} represents normalized Voc. Light harvesting efficiency (LHE) is an important parameter for improving short-circuit current density (J_{sc}) and determining efficiency of QDSCs. A higher LHE leads to greater efficiency. LHE, also known as absorptance (A), It refers to the proportion of light energy taken in at a specific wavelength in dye-sensitized solar cells (DSSCs) or QDSCs [52].

$$LHE = A = \frac{I_{abs}}{I_o} \tag{4}$$

Herein, incident and absorbed intensity are represented by I_o and I_{abs}, respectively. J_{sc} refers to the current density of a solar cell when there is no voltage applied across it and is determined by Eq. (5).

$$J_{sc} = \int_o^\infty q A(E) I_{sun}(E) dE \tag{5}$$

Here I_{sun} (E) and q are photon flux density (AM1.5G spectrum) and electron charge, respectively. The parameter J_{sc} depends on various factors like solar cell area, spectrum of incident light, material's optical properties etc. In this computation, E_{CB} of TiO_2 is considered −4.0 eV [53].

3. Results and discussion

3.1. Assessment of structural characteristics of both undoped and doped GQDs

To comprehend reasoning behind our computations, we initially examined characteristics and structure of GQDs prior to and following introduction of B, Cl, and F atoms through substitutional doping. We created a model of an electron-donating coronene molecule as a GQD, with edges capped by a couple of CO_2H groups, and referred to it as "CO_2H-GQD". This model will facilitate electron transfer from donor (GQD) to acceptor (titanium dioxide) surface when exposed to light. Absorption of a photon will result in an increase in electron energy from GQD's ground state to its excited state, or CB of TiO_2. Excited electron is injected in CB of titanium dioxide via various mechanisms, such as adiabatic or non-adiabatic processes. Fine-tuned geometries of CO_2H-GQD (coronene) with 3 substitutional adsorbed atoms are displayed in Fig. 1. Carbon-Carbon bond distance in CO_2H-GQD is approximately 1.43 Å, while C-O bond distance in benzene rings connected to CO_2H groups typically is between 1.209 and 1.217 Å and C-C bond distance is between 1.49 and 1.52 Å [54]. Additionally, optimized bond angle between C atoms in CO_2H-GQD is 122.19°. Nevertheless, angle is raised by
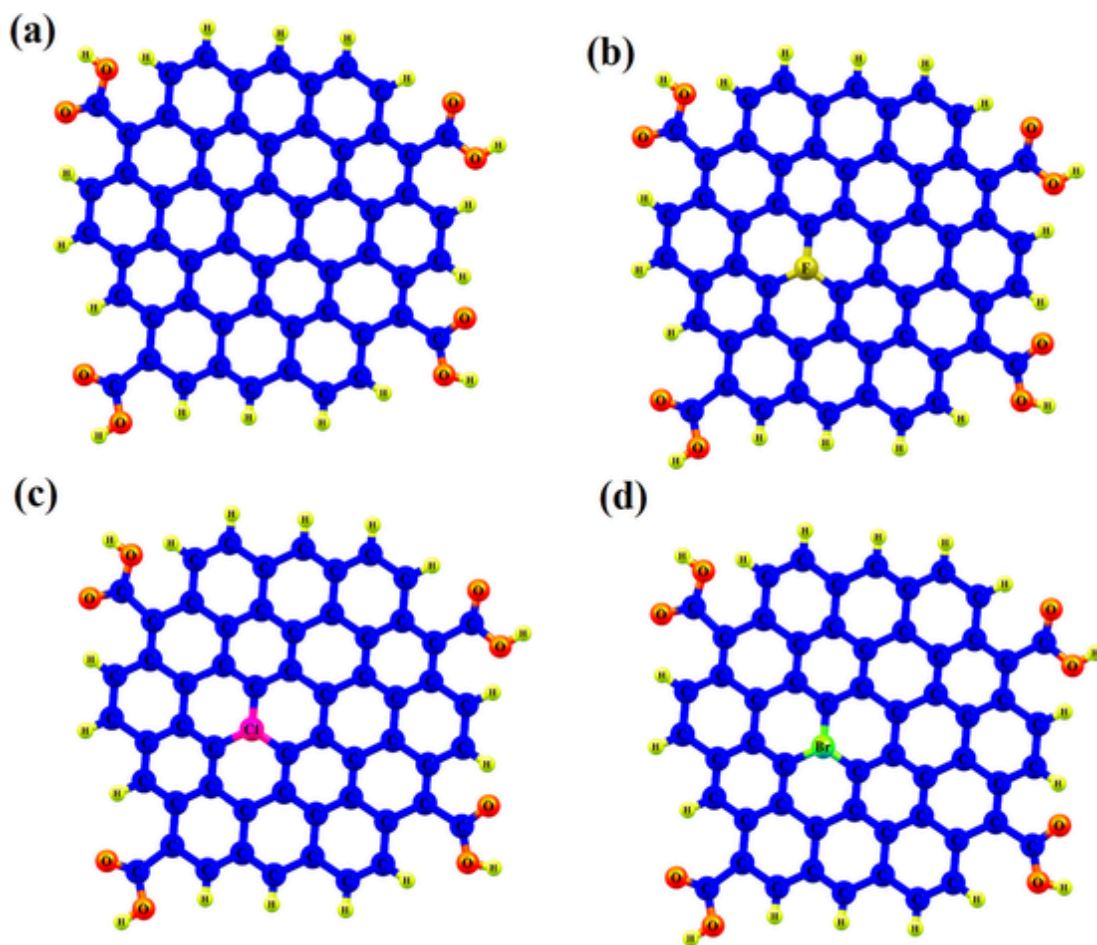
Fig.1. Fine-tuned structures of (a) CO_2H edge-functionalized graphene quantum dot, (b) F@CO_2H-GQD (c) Cl@CO_2H-GQD (d) Br@CO_2H-GQD.

1.95° because of repulsion between benzene ring and carboxyl group. Also, in the FTIR spectrum analysis, none of the samples showed any imaginary vibrational frequencies in Fig. 1S, indicating the stability of the structures.

According to figure, impact of substitutional doping in CO_2H-GQD is evident. When the F atom is introduced (as shown in Fig. 2(b)), bond distance of C-F in Al@CO_2H-GQDs has been computed to be 1.39 Å. Likewise, when Cl atom is introduced (as depicted in Fig. 2(c)), C-Cl
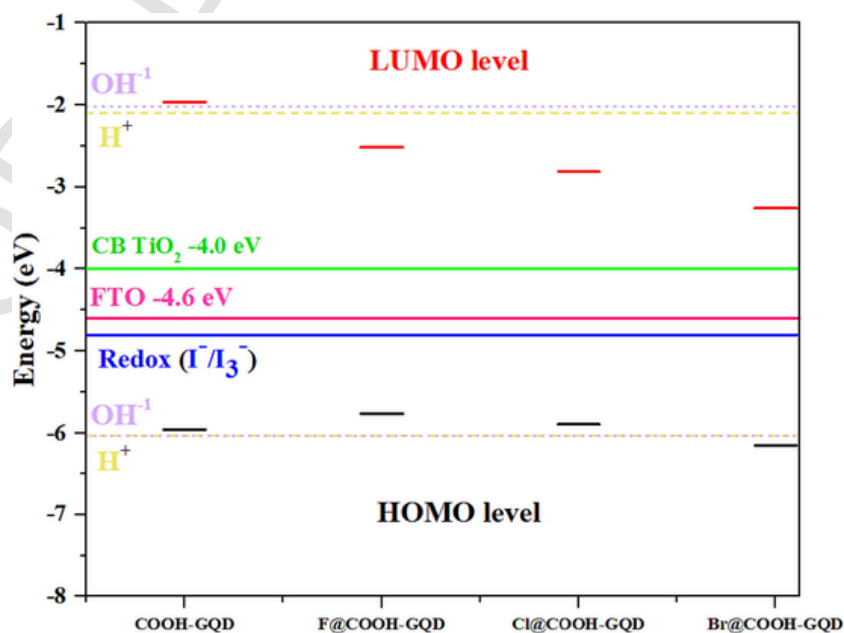
Fig.2. LUMO and HOMO diagrams of both undoped and doped CO_2H edge-functionalized graphene quantum dots.

bond distance in Cl@CO$_2$H-GQDs has been computed to be 1.76 Å. Our computed bond lengths between C-Cl and C-Br align with previously reported findings [55,56]. Variation in bond lengths between Cl, F, and C can be explained by atomic radii of these them. Meanwhile, Br doping in CO$_2$H-GQD (as illustrated in Fig. 2(d)) distorts hexagonal ring, resulting in C-Br bond distance of approximately 1.96 Å. This structural alteration in GQD is because inclusion of these adsorbed atoms disrupts sp^2 hybridization of C atoms, leading to considerable alterations in electronic attributes of CO$_2$H-GQD. Additionally, binding energy values (E$_b$) of CO$_2$H-GQD and doped CO$_2$H-GQD were computed to assess stability of various structures. E$_b$ values of both undoped and doped CO$_2$H-GQD are computed as:

$$\text{undoped}:$$
$$E_b = \frac{\left[nE_{(O)} + nE_{(H)} + nE_{(C)} - E_{CO_2H-GQD} \right]}{N}$$
$$\text{doped}:$$
$$E_b = \frac{\left[nE_{(x)} + nE_{(O)} + nE_{(H)} + nE_{(C)} - E_{x@CO_2H-GQD} \right]}{N} \quad (7)$$

Herein, energy values of one atom of O, H, and C are represented by E$_{(O)}$, E$_{(H)}$ and E$_{(C)}$, respectively. Also, number of atoms in all considered system, as well as total energy of doped/undoped systems are represented by n, E$_{(CO2H-GQD)}$ and E$_{(x@COOH-GQD)}$, respectively. E$_b$ values of undoped and doped CO$_2$H-GQD are listed in Table 1. E$_b$ per atom of CO$_2$H-GQD is 3.98 eV, and this value increases further for doped systems. Table 1 shows that all E$_b$ values are positive, indicating that all structures are stable. The fact that all doped systems have similar E$_b$ values can be explained by their structural attributes, as their ionic radii are almost the same and there is minimal alteration in bond distances between carbon–fluorine and carbon-chlorine. Nevertheless, for Br doping, there is a slight distortion in hexagonal ring which results in a change in bond distance from ~1.43 to 1.96 Å, leading to a lower E$_b$ of 5.36 eV. Total dipole moment for all undoped and doped CO$_2$H-GQD is also revealed in Table 1. Doping in CO$_2$H-GQD increases total dipole moment, and the highest dipole moment of 3.95 Debye is observed in bromide-doped CO$_2$H-GQD. This can be attributed to structure alteration, which generates differences between local dipoles. Reason for increased dipole moment in Br-doped graphene quantum dot can be traced back to distortion of hexagonal structure next to Br atom in CO$_2$H-GQD. When Br atom is added to CO$_2$H-GQD, it breaks symmetry in π-electrons of graphene quantum dot, leading to an increase in dipole moment compared to other doped systems. Increment in dipole moment due to mechanical contortion is because of broken symmetry. Additionally, differing electronegativity values of bromide and carbon cause charge redistribution, which contributes to formation of dipole moment [57]. The results in Table 1S show that the doping of the F, Cl, and Br atoms in GQD led to a decrease in the enthalpy of solvation and an increase in the Gibbs free energy of solvation. The addition of the F

atom resulted in the largest decrease in the enthalpy of solvation among the three atoms considered. This can be attributed to the fact that the F atom is the most electronegative of the three atoms and forms stronger interactions with the solvent, leading to a more favorable solvation process. In contrast, the addition of the Cl and Br atoms resulted in a smaller decrease in the enthalpy of solvation compared to the F atom. This can be explained by the fact that the electronegativity of Cl and Br are lower than that of F. In other words, the results indicate that the inclusion of highly electronegative atoms such as F can significantly improve the solubility of GQD in solvents, while the inclusion of less electronegative atoms such as Cl and Br may have a more limited effect.

3.2. Assessing electronic characteristics

Computed HOMO-LUMO gap (E$_g$) and HOMO-LUMO energies for all systems considered are displayed in Table 1. Impact of adatoms over electronic attributes is evident from alteration in LUMO and HOMO energies presented in Fig. 2 and Table 1. There is a noticeable difference in LUMO and HOMO energy levels as well as in E$_g$, as indicated by computed values in Table 1. Doping adsorbed atoms results in a reduction of band gap. Band gap of considered systems follows a specific order: Br@CO$_2$H-GQD has the smallest band gap of 2.89 eV, followed by Cl@CO$_2$H-GQD with 3.08 eV, then F@CO$_2$H-GQD with 3.24 eV, and finally CO$_2$H-GQD with the largest band gap of 3.99 eV. The data presented in Fig. 2 indicates that LUMO energy values of whole doped and undoped CO$_2$H-GQDs are higher than CB of titanium dioxide (−4.0 eV) [58], suggesting efficient injection of electrons from excited states of undoped and doped systems into CB of titanium dioxide. Additionally, HOMO energy values of systems are lower than I$^-$/I^{3-} (−4.8 eV) [59], indicating that regeneration might occur rapidly and effectively. To enable hole transfer from QDs to the electrolyte, it is established that the HOMO energy of X-doped CO$_2$H-GQDs should exceed the valence bands of the GQDs. All doped systems have energy level arrangements that are suitable in comparison to those of the GQDs, thus demonstrating the effective injection of holes from QDs into the doped system. The Br doped with the deepest HOMO energy level is potentially the optimal dopant for QDSSCs but further evaluations of additional properties are necessary to identify the most efficient material.

To comprehend connection between a molecule's structure and its activity, molecular electrostatic potential (MESP) was computed. This potential refers to force that a unit positive charge would feel in proximity to molecule, taking into account its electron density distribution. MESP is indicative of molecule's chemical reactivity, with negative potential indicating sites that are prone to nucleophilic attack and positive potential denoting sites that are susceptible to electrophilic attack. Fig. 3 displays base ring plane MESP of CO$_2$H-GQD systems, both doped and undoped. All the systems analyzed have been projected onto electron density surface of 0.0160 units. Positive electrostatic potential is displayed by blue surface, whereas negative electrostatic potential is illustrated by red-colored surface. MESP potential can be arranged in ascending order as follows: red, orange, yellow, green, and blue, which green color indicating region of zero potential. When Cl and Br are introduced, carboxyl group of GQD (coronene) has a tendency to exhibit an electrostatic potential that is more negative than before. This makes it a more suitable option for electron injection.

In order to examine impact of doping on electronic characteristics of CO$_2$H-GQD, we computed work function (WF) of both doped and undoped CO$_2$H-GQD, which is the least amount of energy that an electron in the highest occupied level requires to escape from solid in a field-free area at thermodynamic temperature. It is determined using formula below [60]:

$$WF = \frac{I + A}{2} \quad (8)$$

Table 1
Computed parameters for solar cells under consideration, including work function (WF), electron affinity (EA), and HOMO-LUMO energy gap (E$_g$), as well as energy values of LUMO and HOMO.

Parameter	CO$_2$H-GQD	F@CO$_2$H-GQD	Cl@CO$_2$H-GQD	Br@CO$_2$H-GQD
E$_{HOMO}$ (eV)	−5.96	−5.76	−5.89	−6.15
E$_{LUMO}$ (eV)	−1.97	−2.52	−2.81	−3.26
E$_g$ (eV)	3.99	3.24	3.08	2.89
E$_b$ (eV)	5.23	6.02	5.87	5.36
D (Debye)	2.26	2.80	3.69	3.95
EA	1.97	2.52	2.81	3.26
WF	3.96	4.14	4.35	4.71
I (eV)	5.96	5.76	5.89	6.15
A (eV)	1.97	2.52	2.81	3.26
η (eV)	2.00	1.62	1.54	1.45
µ (eV)	3.97	4.14	4.35	4.71
ω (eV)	3.94	5.29	6.14	7.66

Fig.3. MESP diagrams of both undoped and doped CO_2H edge-functionalized graphene quantum dots.

In this context, electron affinity (A) and ionization energy (I) are represented using energies of HOMO and LUMO, where IE is equal to negative value of HOMO and EA is equal to negative value of LUMO. Work function of CO_2H-GQD experiences a considerable shift after the introduction of dopants. Work function of CO_2H-GQD without dopants has been computed as 4.41 eV, and it remains relatively constant even after introduction of F. However, work function increases slightly with Cl doping, and a notable change is observed with Br doping, as it significantly raises work function of CO_2H-GQD. These computed WF values are presented in Table 1. Modification in WF can be explained by charge transfer between dopants and CO_2H-GQD.

Table 1 contains the quantum molecular descriptors of all the samples that were calculated, illustrating their electronic traits and chemical reactivities. One can determine the stability and structural reactivity of a material using its global chemical potential (μ), electronegativity (χ), and hardness (η). These properties can be calculated with the help of the equations $\mu = -(I + A)/2$, $\chi = (I + A)/2$, and $\eta = (I-A)/2$, respectively [61]. In general, a material with smaller values of μ, η, and E_g indicates easier charge transport and higher chemical reactivity. Furthermore, a molecule that has a higher electrophilicity index ($\omega = \mu^2/2\eta$) can be considered to possess superior electrophilic properties. The ionization potential (I) of a GQD can affect its hole injection ability. A smaller I generally imply an enhanced hole injection capability. Among the samples tested, the GQD with the electron-withdrawing Br substituent has the largest I value of 6.15 eV. Meanwhile, the F-doped GQD has the smallest I value of 5.76 eV. This suggests that the F-doped GQD might hold the greatest potential to be used in QDSSCs due to its superior hole injection capability. The chemical stability of a material

is often associated with its hardness (η), which is a measure of its resistance to corrosion. The η values shown in Table 1 increase as X changes from undoped > F > Cl > Br. This indicates that the incorporation of electron-donating substituents decreases the stability of the GQD, while the undoped GQD has the highest stability.

3.3. Solar cell parameters and optical features

Table 2 and Fig. 2S displays maximum wavelength absorption observed in UV–vis spectra for CO_2H-GQD, both undoped and doped, at 10 distinct excited states in H_2O solvent. The identical level of theory was utilized for both. To achieve greater photon harvesting, absorption spectra of all donors, including CO_2H-GQD and x@CO_2H-GQD, must be similar to that of solar spectra. For whole systems analyzed, it has been observed that absorption occurs only within visible regions. Nature and energy of electronic transitions have been investigated via primary singlet–singlet electron transitions, along with oscillator strength (f) [62], which is presented in Table 2 and indicates potential for absorption

Table 2

Computed values of light harvesting energy (LHE), oscillator strength (f), electronic transition energy (eV), and the highest absorption wavelength, λ_{max} (nm), for whole regarded systems.

Parameter	CO_2H-GQD	F@CO_2H-GQD	Cl@CO_2H-GQD	Br@CO_2H-GQD
λ_{max} (nm)	308	357	371	405
Energy (eV)	3.44	2.48	2.74	2.33
f	0.80	0.35	0.29	0.18
LHE	0.84	0.55	0.49	0.34

and emission during transition between energy levels of LUMO and HOMO [63].

In our closed shell CO2H-GQD, the most significant electronic transitions contributing to maximum peak wavelength and f parameter are H1 → LUMO (17 %) and HOMO → L + 1 (83 %). There are also smaller contributions to the electronic transition from H-2 → L + 2 (4 %) and H-1 → L + 1 (6 %) [38]. Table 2 clearly indicates that absorption attributes of CO_2H-GQD can be modified by doping with Br, Cl, and F. This finding is consistent with previous experimental research [64].

Small deviation from results reported in previous experimental work can be attributed to several factors, such as an unknown concentration of carboxyl groups attached to GQD edges, as well as variations in shape and size. Since GQDs are known to have optical and electronic attributes that are highly dependent on their shape and size, any changes in these attributes can lead to variations in optical attributes and a shift in UV–vis peak [65]. The observed transition can be explained by n → π* transition resulting from presence of C═O. Following the introduction of P, B, and N doping, observed peaks are shifted towards red end of spectrum, in order of CO_2H-GQD (308 nm) < F@CO_2H-GQD (357 nm) < Cl@CO_2H-GQD (371 nm) < Br@CO_2H-GQD (405 nm). This result is consistent with earlier theoretical findings [42]. The observed effect can be attributed to additional valence electrons present in Br and Cl atoms and relatively larger atomic radii, which can lead to modifications in electronic transition features of CO_2H-GQDs. Among all doped CO_2H-GQDs, Br-doped CO_2H-GQD demonstrates the strongest absorption at 405 nm, suggesting that it can harvest more light at longer wavelengths [66]. As a result, PCE of solar cells made with Br-doped CO_2H-GQD can be further increased.

In order to assess their suitability for use in solar cells, we analyzed performance parameters of both doped and undoped CO2H-GQD, including η, FF, J_{sc}, and V_{oc}. In order to produce high-efficiency and cost-effective PV devices for use in solar cells, titanium dioxide photoanodes have been of great interest. Out of whole metal oxides that are used in quantum dot solar cells, titanium dioxide is particularly important due to its ability to collect charges effectively [66]. In addition, TiO_2 is an environmentally friendly, naturally abundant, and affordable material. When graphene quantum dots are synthesized on TiO_2, they facilitate active charge injection from QDs to titanium dioxide material [67]. Moreover, due to their π-electron systems, GQDs can be directly connected to TiO_2, which enhances donor–acceptor junction. Research has shown that electronic coupling between TiO_2 and GQDs can be enhanced via the use of various functional groups [67]. In this work, CO_2H-GQD (donor) is attached to titanium dioxide surface via CO_2H group located at edges, resulting in a high electron injection. Furthermore, we discovered via our analysis of electronic features of doped and undoped CO_2H-GQDs that LUMO energy values for whole systems are greater than CB of titanium dioxide, indicating a rapid electronic injection from excited states of graphene quantum dots to CB of titanium dioxide. HOMO energy values are located under I−/I3−, suggesting a rapid and efficacious regeneration. There have been numerous studies on nanoscale carbon materials (such as graphene, CNTs, and GQDs) with TiO_2, as they have ability to harvest a broad spectrum of solar light and rapidly separate charges [68].

Distinct electronic levels of doped and undoped CO_2H-GQDs facilitate hot electron injection and substantial charge separation on titanium dioxide. When analyzing outcomes for their potential utilization in solar cells that use quantum dots, we concentrated on surface of nanocrystalline titanium dioxide, as LUMO energy values of both doped and undoped CO_2H-GQDs are higher than CB of titanium dioxide, and HOMO energy values of both doped and undoped CO_2H-GQDs are located below I−/I3−. Efficient functioning of QDSCs can be improved by injecting electrons quickly from doped/undoped CO_2H-GQDs on titanium dioxide. Table 2 displays information about light harvesting en-

ergy (LHE), oscillator strength (f), and electronic transition energy for whole systems being considered. Light harvesting energy is determined using equation provided [69]:

$$LHE = 1 - 10^{-f} \qquad (9)$$

Oscillator strength (f) is determined through TD-DFT computations. Systems are ranked in order of their LHE, with CO_2H-GQD having the highest value (0.84), followed by F@CO_2H-GQD (0.55), Cl@CO_2H-GQD (0.49), and Br@CO_2H-GQD (0.34). Although there is only a marginal difference in LHE among doped systems, this will lead to comparable photocurrents in solar cells. The obtained values of LHE in the present work are comparable with the reported values for other compounds usable in quantum dot-based solar cells [70,71]. For example, after halogen doping in spiro-bifluorene based compound, LHE values were obtained in the range of 0.25 to 0.35 [70]. For both doped and undoped CO_2H-GQD, information about solar cell parameters is provided in Table 3. V_{oc} is a key parameter that can be calculated by determining difference between CB of TiO2 and LUMO of donor. V_{oc} of CO_2H-GQD is influenced by LUMO energies of the doped CO_2H-GQD. For all systems analyzed in this study, V_{oc} values were between 0.74 and 2.03 eV. Positive V_{oc} values indicate that transfer of electrons from doped CO_2H-GQD to TiO_2 occurs easily. The highest J_{sc} value was observed in Br@CO_2H-GQD, and the lowest V_{oc} value was related to undoped CO_2H-GQD. Undoped CO_2H-GQD exhibits an efficiency of 1.05 %, an FF of 0.914, and a J_{sc} of 0.59 mA/cm². Efficiency reduces to 0.96 % following introduction of F dopants. Furthermore, efficiency decreases to 0.87 % upon Br doping that could be ascribed to enhanced electron injection over TiO_2 surface. Our findings reveal that CO_2H-GQD doped with F is the most appropriate option for utilization in solar cells.

4. Conclusion

To sum up, theoretical computations have been employed to examine how substitutional doping affects PCE of doped and undoped CO_2-GQDs. Findings demonstrate that doping with F, Cl, and Br atoms can significantly enhance efficiency of CO_2H edge-functionalized GQDs, as these atoms tend to alter optical and electronic attributes of GQDs. Doping also has an impact on energy levels of FMOs and E_g of all the systems under consideration, leading to changes in their photoelectric attributes. E_g values of CO2H-GQD, Br@CO2H-GQD, Cl@CO_2HGQD, and F@CO_2H-GQD have been computed employing DFT/B3LYP/6-31G level and were found to be 3.99, 2.89, 3.08, and 3.24 eV, respectively. Mechanism of binding delivers useful guidelines to design high-performance solar cells. The fact that bromide-doped CO_2H-GQD exhibits the strongest absorption at 405 nm indicates that this system can harvest more light at longer wavelengths. By reducing optical band gap, GQDs can be used in optoelectronics. Computed V_{oc} for TiO_2 of undoped/doped CO_2H-GQD indicate that there is efficient electron injection from donor to acceptor site. Br@CO_2H-GQD exhibits maximum J_{sc} due to its considerable energy levels of HOMO and narrow band gap in comparison to every other system that has been doped, which further impacts photoelectric attributes. Efficiency order, from lowest to highest, is CO_2H-GQD, F@CO_2H-GQD, Cl@CO_2H-GQD, and Br@CO_2H-GQD. F@CO_2H-GQD exhibits the highest efficiency due to both efficient electron injection in TiO_2 and its lower atomic radius. Based on our theoretical computations, the addition of a foreign atom to edge-

Table 3
Computed parameters of solar cell for whole regarded systems.

Parameter	CO_2H-GQD	F@CO_2H-GQD	Cl@CO_2H-GQD	Br@CO_2H-GQD
V_{oc} (eV)	2.03	1.48	1.19	0.74
FF	0.914	0.924	0.926	0.909
J_{sc} (mA/cm²)	0.57	0.70	0.79	0.88
η%	1.09	0.96	0.87	0.59

functionalized GQDs makes them promising candidates for highly efficient QDSCs in next generation.

CRediT authorship contribution statement

Ali A. Rajhi : Writing – review & editing, Software, Methodology, Investigation, Formal analysis. **Karam Myaser Abd Alaziz :** Writing – review & editing, Validation, Methodology, Formal analysis, Data curation, Conceptualization. **Byron Stalin Rojas Oviedo :** Writing – review & editing, Software, Methodology, Investigation, Formal analysis. **Anupam Yadav :** Writing – original draft, Supervision, Methodology, Investigation, Formal analysis. **Eduardo Hernández :** Writing – review & editing, Writing – original draft, Investigation, Formal analysis, Data curation. **César Gallegos :** Writing – review & editing, Writing – original draft, Validation, Software, Methodology, Investigation. **Sagr Alamri :** Writing – review & editing, Writing – original draft, Visualization, Validation, Formal analysis, Data curation. **Alaauldeen A. Duhduh :** Writing – review & editing, Validation, Methodology, Investigation, Formal analysis, Data curation.

Declaration of Competing Interest

The authors declare that they have no known competing financial interests or personal relationships that could have appeared to influence the work reported in this paper.

Data availability

No data was used for the research described in the article.

Acknowledgments

Appendix A. Supplementary data

Supplementary data to this article can be found online at https://doi.org/10.1016/j.jphotochem.2023.115240.

References

[1] A.A. Asif, R. Singh, G.F. Alapatt, Technical and economic assessment of perovskite solar cells for large scale manufacturing, J. Renewable Sustainable Energy 7 (2015).
[2] F.H. Isikgor, S. Zhumagali, L.V.T. Merino, M. De Bastiani, I. McCulloch, S. De Wolf, Molecular engineering of contact interfaces for high-performance perovskite solar cells, Nat. Rev. Mater. 8 (2023) 89–108.
[3] A. Wang, M. He, M.A. Green, K. Sun, X. Hao, A critical review on the progress of kesterite solar cells: current strategies and insights, Adv. Energy Mater. 13 (2023) 2203046.
[4] M.K. Hossain, D. Samajdar, R.C. Das, A. Arnab, M.F. Rahman, M. Rubel, M.R. Islam, H. Bencherif, R. Pandey, J. Madan, Design and simulation of Cs2BiAgI6 double perovskite solar cells with different electron transport layers for efficiency enhancement, Energy Fuel 37 (2023) 3957–3979.
[5] C. Li, X. Wang, E. Bi, F. Jiang, S.M. Park, Y. Li, L. Chen, Z. Wang, L. Zeng, H. Chen, Rational design of Lewis base molecules for stable and efficient inverted perovskite solar cells, Science 379 (2023) 690–694.
[6] J. Luo, H. Han, X. Wang, X. Qiu, B. Liu, Y. Lai, X. Chen, R. Zhong, L. Wang, C. Wang, Single-atom Nb anchored on graphitic carbon nitride for boosting electron transfer towards improved photocatalytic performance, Appl. Catal. B 328 (2023) 122495.
[7] H.-X. Zhang, P.-F. Wang, C.-G. Yao, S.-P. Chen, K.-D. Cai, F.-N. Shi, Recent advances of ferro-/piezoelectric polarization effect for dendrite-free metal anodes, Rare Met. (2023) 1–29.
[8] X. Zhang, Y. Tang, F. Zhang, C.S. Lee, A novel aluminum–graphite dual-ion battery, Adv. Energy Mater. 6 (2016) 1502588.
[9] O.E. Semonin, J.M. Luther, S. Choi, H.-Y. Chen, J. Gao, A.J. Nozik, M.C. Beard, Peak external photocurrent quantum efficiency exceeding 100% via MEG in a quantum dot solar cell, Science 334 (2011) 1530–1533.
[10] M.R. Kim, D. Ma, Quantum-dot-based solar cells: recent advances, strategies, and challenges, J. Phys. Chem. Lett. 6 (2015) 85–99.
[11] V. Sharma, B. Roondhe, S. Saxena, A. Shukla, Role of functionalized graphene quantum dots in hydrogen evolution reaction: A density functional theory study, Int. J. Hydrogen Energy 47 (2022) 41748–41758.
[12] S.E. Özönder, C. Ünlü, C. Güleryüz, L. Trabzon, Doped graphene quantum dots UV–vis absorption spectrum: a high-throughput TDDFT Study, ACS Omega, (2023).
[13] X. Kong, J. Zhang, L. Meng, C. Sun, X. Jiang, J. Zhang, C. Zhu, G. Sun, J. Li, X. Li, Low-cost and high-performance polymer solar cells with efficiency insensitive to active-layer thickness, CCS Chem. (2023) 1–11.
[14] Y. Shao, Y. Gao, R. Sun, M. Zhang, J. Min, A versatile and low-cost polymer donor based on 4-chlorothiazole for highly efficient polymer solar cells, Adv. Mater. 35 (2023) 2208750.
[15] X. Kong, J. Zhang, L. Meng, C. Sun, S. Qin, C. Zhu, J. Zhang, J. Li, Z. Wei, Y. Li, 18.55% Efficiency polymer solar cells based on a small molecule acceptor with alkylthienyl outer side chains and a low-cost polymer donor PTQ10, CCS, Chemistry 5 (2023) 841–850.
[16] Q. Liao, S. Li, F. Xi, Z. Tong, X. Chen, X. Wan, W. Ma, R. Deng, High-performance silicon carbon anodes based on value-added recycling strategy of end-of-life photovoltaic modules, Energy 281 (2023) 128345.
[17] H. Xia, L. Zan, P. Yuan, G. Qu, H. Dong, Y. Wei, Y. Yu, Z. Wei, W. Yan, J.S. Hu, Evolution of stabilized 1T-MoS2 by atomic-interface engineering of 2H-MoS2/Fe–Nx towards enhanced sodium ion storage, Angew. Chem. 135 (2023) e202218282.
[18] W. Hao, J. Xie, Reducing diffusion-induced stress of bilayer electrode system by introducing pre-strain in lithium-ion battery, J. Electrochem. Energy Convers. Storage 18 (2021) 020909.
[19] J. Xie, X. Wei, X. Bo, P. Zhang, P. Chen, W. Hao, M. Yuan, State of charge estimation of lithium-ion battery based on extended Kalman filter algorithm, Front. Energy Res. 11 (2023).
[20] E.M. Barea, M. Shalom, S. Giménez, I. Hod, I. Mora-Seró, A. Zaban, J. Bisquert, Design of injection and recombination in quantum dot sensitized solar cells, J. Am. Chem. Soc. 132 (2010) 6834–6839.
[21] R.S. Selinsky, Q. Ding, M.S. Faber, J.C. Wright, S. Jin, Quantum dot nanoscale heterostructures for solar energy conversion, Chem. Soc. Rev. 42 (2013) 2963–2985.
[22] P. Cui, Y. Xue, Sulfication-induced non-radiative electron-hole recombination dynamics in graphene quantum dots for tuning photocatalytic performance, Spectrochim. Acta A Mol. Biomol. Spectrosc. 287 (2023) 122117.
[23] D. He, M. Zeng, Z. Zhang, Y. Bai, G. Xing, H.M. Cheng, Y. Lin, Exciton diffusion and dissociation in organic and quantum-dot solar cells, SmartMat (2023) e1176.
[24] J. Liu, J. Wang, Y. Liu, K. Zhou, J. Wu, S. Li, W. Zhao, Z. Zhou, L. Ye, Toward efficient hybrid solar cells comprising quantum dots and organic materials: progress, strategies, and perspectives, J. Mater. Chem. A 11 (2023) 1013–1038.
[25] Y. Rui, Z. Jin, X. Fan, W. Li, B. Li, T. Li, Y. Wang, L. Wang, J. Liang, Defect passivation and electrical conductivity enhancement in perovskite solar cells using functionalized graphene quantum dots, Mater. Fut. 1 (2022) 045101.
[26] S. Du, H. Xie, J. Yin, Y. Sun, Q. Wang, H. Liu, W. Qi, C. Cai, G. Bi, D. Xiao, Giant hot electron thermalization via stacking of graphene layers, Carbon 203 (2023) 835–841.
[27] X.-M. Huang, N. Chen, D.-N. Ye, A.-G. Zhong, H. Liu, Z. Li, S.-Y. Liu, Structurally complementary star-shaped unfused ring electron acceptors with simultaneously enhanced device parameters for ternary organic solar cells, Solar RRL (2023).
[28] S. Mu, Q. Liu, P. Kidkhunthod, X. Zhou, W. Wang, Y. Tang, Molecular grafting towards high-fraction active nanodots implanted in N-doped carbon for sodium dual-ion batteries, Natl. Sci. Rev. 8 (2021) nwaa178.
[29] S.K. Muzakir, N. Alias, M.M. Yusoff, R. Jose, On the missing links in quantum dot solar cells: a DFT study on fluorophore oxidation and reduction processes in sensitized solar cells, PCCP 15 (2013) 16275–16285.
[30] T. Sogabe, Q. Shen, K. Yamaguchi, Recent progress on quantum dot solar cells: a review, J. Photonics Energy 6 (2016) 040901.
[31] M. Kouhnavard, S. Ikeda, N. Ludin, N.A. Khairudin, B. Ghaffari, M. Mat-Teridi, M. Ibrahim, S. Sepeai, K. Sopian, A review of semiconductor materials as sensitizers for quantum dot-sensitized solar cells, Renew. Sustain. Energy Rev. 37 (2014) 397–407.
[32] S. Bak, D. Kim, H. Lee, Graphene quantum dots and their possible energy applications: A review, Curr. Appl Phys. 16 (2016) 1192–1201.
[33] Z. Pan, H. Rao, I. Mora-Seró, J. Bisquert, X. Zhong, Quantum dot-sensitized solar cells, Chem. Soc. Rev. 47 (2018) 7659–7702.
[34] M. Ebrahimi, V. Soleimanian, M. Ghasemi, M. Nekoeinia, A. Mokhtari, Effects of graphene quantum dots on microstructure, optical and gas sensing properties of coral-like ZnCo2O4 nanoparticles, Phys. B Condens. Matter 650 (2023) 414439.
[35] R. Ren, F. Lai, X. Lang, L. Li, C. Yao, K. Cai, Efficient sulfur host based on Sn doping to construct Fe2O3 nanospheres with high active interface structure for lithium-sulfur batteries, Appl. Surf. Sci. 613 (2023) 156003.
[36] M. Wang, C. Jiang, S. Zhang, X. Song, Y. Tang, H.-M. Cheng, Reversible calcium alloying enables a practical room-temperature rechargeable calcium-ion battery with a high discharge voltage, Nat. Chem. 10 (2018) 667–672.
[37] L. Li, S. Jia, M. Cao, Y. Ji, H. Qiu, D. Zhang, Research progress on transition metal sulfide-based materials as cathode materials for zinc-ion batteries, J. Storage Mater. 67 (2023) 107614.
[38] D. Sharma, R. Jha, S. Kumar, Quantum dot sensitized solar cell: recent advances and future perspectives in photoanode, Sol. Energy Mater. Sol. Cells 155 (2016) 294–322.
[39] M. Bacon, S.J. Bradley, T. Nann, Graphene quantum dots, Part. Part. Syst. Char. 31 (2014) 415–428.
[40] Y.-Q. Zhang, D.-K. Ma, Y.-G. Zhang, W. Chen, S.-M. Huang, N-doped carbon

quantum dots for TiO2-based photocatalysts and dye-sensitized solar cells, Nano Energy 2 (2013) 545–552.

[41] H. Wang, P. Sun, S. Cong, J. Wu, L. Gao, Y. Wang, X. Dai, Q. Yi, G. Zou, Nitrogen-doped carbon dots for "green" quantum dot solar cells, Nanoscale Res. Lett. 11 (2016) 1–6.

[42] J. Feng, H. Dong, B. Pang, F. Shao, C. Zhang, L. Yu, L. Dong, Theoretical study on the optical and electronic properties of graphene quantum dots doped with heteroatoms, PCCP 20 (2018) 15244–15252.

[43] J. Beheshtian, A.A. Peyghan, Z. Bagheri, Detection of phosgene by Sc-doped BN nanotubes: a DFT study, Sens. Actuators B 171 (2012) 846–852.

[44] M.A. Abdulsattar, SiGe superlattice nanocrystal pure and doped with substitutional phosphorus single atom: Density functional theory study, Superlattice. Microst. 50 (2011) 377–385.

[45] D. Xie, M. Zhang, Q. Liu, Y. Lin, A. Yu, Y. Tang, Organic-Inorganic Conformal Extending High-Purity Metal Nanosheets for Robust Electrochemical Lithium-Ion Storage, Adv. Funct. Mater. (2023) 2306291.

[46] M.W. Schmidt, K.K. Baldridge, J.A. Boatz, S.T. Elbert, M.S. Gordon, J.H. Jensen, S. Koseki, N. Matsunaga, K.A. Nguyen, S. Su, General atomic and molecular electronic structure system, J. Comput. Chem. 14 (1993) 1347–1363.

[47] G. Scalmani, M.J. Frisch, Continuous surface charge polarizable continuum models of solvation. I. General formalism, J. Chem. Phys. 132 (2010).

[48] T. Lu, F. Chen, Multiwfn: A multifunctional wavefunction analyzer, J. Comput. Chem. 33 (2012) 580–592.

[49] E. Cancès, B. Mennucci, J. Tomasi, A new integral equation formalism for the polarizable continuum model: Theoretical background and applications to isotropic and anisotropic dielectrics, J. Chem. Phys. 107 (1997) 3032–3041.

[50] L. Yu, A. Zunger, Identification of potential photovoltaic absorbers based on first-principles spectroscopic screening of materials, Phys. Rev. Lett. 108 (2012) 068701.

[51] W.-J. Yin, T. Shi, Y. Yan, Unique properties of halide perovskites as possible origins of the superior solar cell performance, Adv. Mater. 26 (2014) 4653–4658.

[52] A. Lonergan, C. O'Dwyer, Many facets of photonic crystals: from optics and sensors to energy storage and photocatalysis, Adv. Mater. Technol. 8 (2023) 2201410.

[53] D. Cahen, G. Hodes, M. Grätzel, J.F. Guillemoles, I. Riess, Nature of photovoltaic action in dye-sensitized solar cells, J. Phys. Chem. B 104 (2000) 2053–2059.

[54] M. Barańska, K. Chruszcz, B. Boduszek, L.M. Proniewicz, FT-IR and FT-Raman study of selected pyridinephosphonocarboxylic acids, Vib. Spectrosc 31 (2003) 295–311.

[55] H.-H. Huang, A. Anand, C.-J. Lin, H.-J. Lin, Y.-W. Lin, S.G. Harroun, C.-C. Huang, LED irradiation of halogen/nitrogen-doped polymeric graphene quantum dots triggers the photodynamic inactivation of bacteria in infected wounds, Carbon 174 (2021) 710–722.

[56] S. Kaushal, M. Kaur, N. Kaur, V. Kumari, P.P. Singh, Heteroatom-doped graphene as sensing materials: A mini review, RSC Adv. 10 (2020) 28608–28629.

[57] J. Beheshtian, A. Sadeghi, M. Neek-Amal, K.H. Michel, F.M. Peeters, Induced polarization and electronic properties of carbon-doped boron nitride nanoribbons, Phys. Rev. B 86 (2012) 195433.

[58] D. Cahen, G. Hodes, M. Graetzel, J.F. Guillemoles, I. Riess, Nature of photovoltaic action in dye-sensitized solar cells, J. Phys. Chem. B 104 (2000) 2053–2059.

[59] A.G. Al-Sehemi, A. Irfan, A.M. Asiri, Y.A. Ammar, Synthesis, characterization and DFT study of methoxybenzylidene containing chromophores for DSSC materials, Spectrochim. Acta A Mol. Biomol. Spectrosc. 91 (2012) 239–243.

[60] V. Sharma, P.K. Jha, Enhancement in power conversion efficiency of edge-functionalized graphene quantum dot through adatoms for solar cell applications, Sol. Energy Mater. Sol. Cells 200 (2019) 109908.

[61] V. Zaverkin, J. Kästner, Gaussian moments as physically inspired molecular descriptors for accurate and scalable machine learning potentials, J. Chem. Theory Comput. 16 (2020) 5410–5421.

[62] A. Hlel, A. Mabrouk, M. Chemek, I.B. Khalifa, K. Alimi, A DFT study of charge-transfer and opto-electronic properties of some new materials involving carbazole units, Comput. Condens. Matter 3 (2015) 30–40.

[63] W. Demtröder, W. Demtröder, Nonlinear Spectroscopy, Springer, 2003.

[64] D. Bhatnagar, S. Singh, S. Yadav, A. Kumar, I. Kaur, Experimental and theoretical investigation of relative optical band gaps in graphene generations, Mater. Res. Express 4 (2017) 015101.

[65] P. Tian, L. Tang, K. Teng, S. Lau, Graphene quantum dots from chemistry to applications, Mater. Today Chem. 10 (2018) 221–258.

[66] N. Santhanamoorthi, C.-M. Lo, J.-C. Jiang, Molecular design of porphyrins for dye-sensitized solar cells: a DFT/TDDFT study, J. Phys. Chem. Lett. 4 (2013) 524–530.

[67] R. Long, D. Casanova, W.-H. Fang, O.V. Prezhdo, Donor–acceptor interaction determines the mechanism of photoinduced electron injection from graphene quantum dots into TiO2: π-stacking supersedes covalent bonding, J. Am. Chem. Soc. 139 (2017) 2619–2629.

[68] Z. Salam, E. Vijayakumar, A. Subramania, N. Sivasankar, S. Mallick, Graphene quantum dots decorated electrospun TiO2 nanofibers as an effective photoanode for dye sensitized solar cells, Sol. Energy Mater. Sol. Cells 143 (2015) 250–259.

[69] M. Xie, J. Wang, H.-Q. Xia, F.-Q. Bai, R. Jia, J.-G. Rim, H.-X. Zhang, Theoretical studies on the spectroscopic properties of porphyrin derivatives for dye-sensitized solar cell application, RSC Adv. 5 (2015) 33653–33665.

[70] Z. Shariatinia, Designing novel spiro compounds as favorable hole transport materials for quantum dot sensitized photovoltaics, Sol. Energy 236 (2022) 548–560.

[71] Z. Shariatinia, Hole transport properties of some spiro-based materials for quantum dot sensitized solar devices, J. Photochem. Photobiol. A Chem. 427 (2022) 113810.